Supplemental material: Transient thermal characterization of suspended monolayer MoS_2

Robin J. Dolleman,[1,*] David Lloyd,[2] Martin Lee,[1] J. Scott Bunch,[2,3] Herre S. J. van der Zant,[1] and Peter G. Steeneken[1,4]

[1] *Kavli Institute of Nanoscience, Delft University of Technology, Lorentzweg 1, 2628 CJ, Delft, The Netherlands*
[2] *Department of Mechanical Engineering, Boston University, Boston, Massachusetts 02215 United States*
[3] *Boston University, Division of Materials Science and Engineering, Brookline, Massachusetts 02446 United States*
[4] *Department of Precision and Microsystems Engineering, Delft University of Technology, Mekelweg 2, 2628 CD, Delft, The Netherlands*

COMSOL MODEL

Here we show the COMSOL model used to derive the expression for τ used in the main section of the paper. An analytic expression was derived for the thermal time constant τ in the case of a uniformly heated circular disk[1]:

$$\tau = \frac{a^2 \rho c_p}{\mu^2 k}, \tag{1}$$

where a is the drum radius, ρ the density, c_p the specific heat, k the thermal conductivity the material and $\mu = 2.4048$ is the first root of the Bessel function $J_0(x)$. Since the experiment uses a laser spot with a size that is much smaller than the drum diameter to heat the drum, equation 1 needs to be modified in order to accurately describe the time constant of the system. Our approach is to choose a fixed value of the specific heat $c_p = 373.5$ J/(kg·K) and vary both a and k to find a new value of μ that will enable us to accurately determine the value of k or the thermal diffusivity α from the experiment.

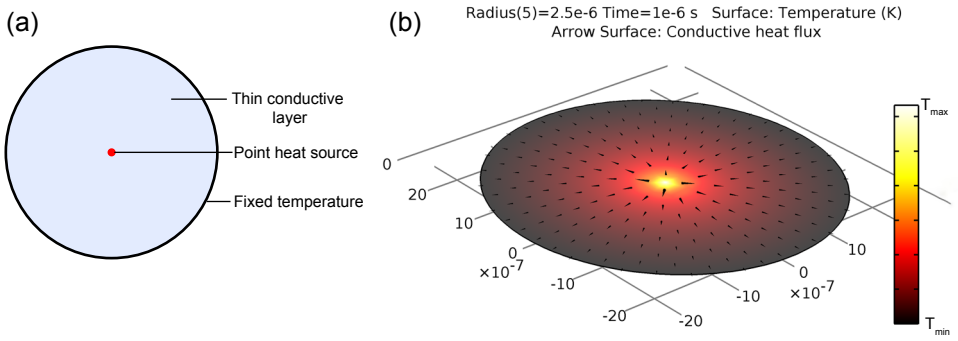

FIG. 1. (a) Schematic drawing of the simulation. (b) Temperature profile at the end of the simulation for a 5-micron diameter drum.

Figure 1 shows the setup of the COMSOL simulation in order to find the thermal time constant τ. A simple circular domain was defined and the heat transport is simulated using the "heat transport in thin shells" module. A point source in the center was used to simulate the heat flux and the boundaries of the domain were kept at a fixed temperature.

In order to find the time constant τ, a time-dependent simulation was performed that simulates the response to a step function in the heat source. The resulting time dependent temperature increase was calculated by taking the average over the entire domain. This results in the time-dependent traces shown in Fig. 2. For each trace, the time constant is found by fitting:

$$T(t) = T_0 + T_{\text{end}} \exp\left(-t/\tau\right). \tag{2}$$

The diameter-dependence is simulated using a range of values of k, we selected a suitable range by selecting values found in literature. It is found that for the range between $10 < k < 100$ we find values of $\mu^2 \approx 5.0$. This model is shown as solid lines in Fig. 3. We find that $\mu^2 = 5.0$ yields good agreement at the higher values of k. Low values of k results in larger deviations at larger diameters, which can also be attributed to the a^2 dependence of τ. From this model, we find that the value of τ with $\mu^2 = 5.0$ should produce the correct value of k or α within 10% error as long as $15 < k < 100$ W/(m·K) and $2a \leq 8$ μm.

ADDITIONAL DISCUSSION ON CROSSTALK

Here we discuss the identification of the electrical cross-talk in the experiments. In Fig. 4 we measure a single layer graphene resonator since these drums do not break at higher laser powers. The left figure shows the frequency response at the same DC laser powers and modulation current as used in the experiments with MoS_2. The electrical crosstalk is more prominently visible since the MoS_2 drums show a much stronger amplitude of the signal compared to graphene. Increasing the laser power by a factor of 3 by changing the neutral density filter after the blue laser, gives the frequency response to the right. This shows that the feature between 100 kHz and 1MHz almost fully disappears, from which we conclude that this feature cannot be attributed to the mechanical motion of the drum.

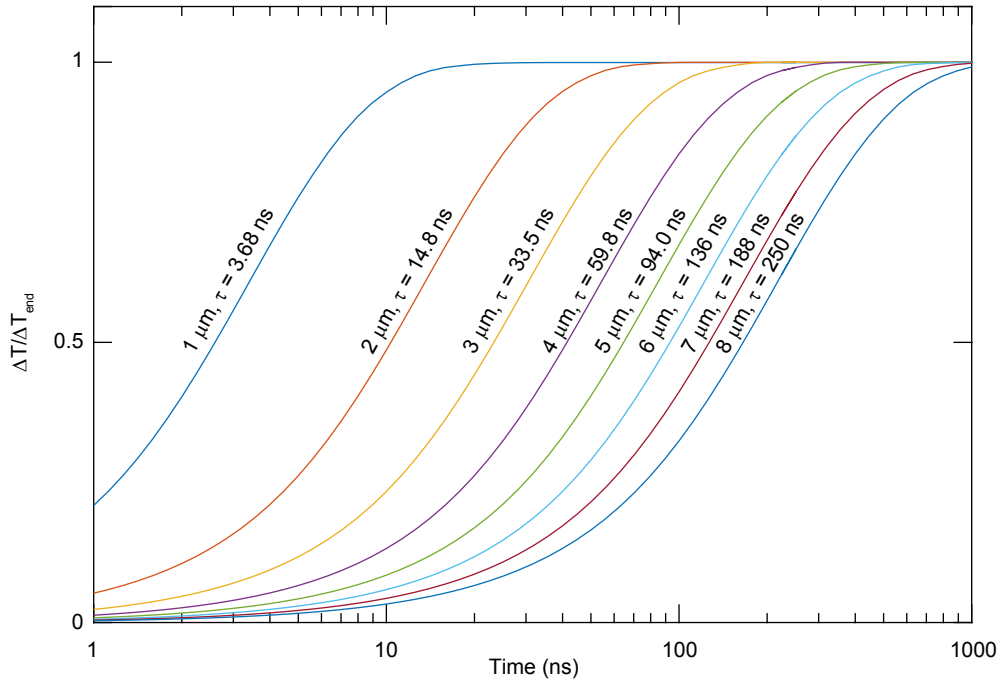

FIG. 2. Simulated temperature as function of time, from which τ can be derived for different diameters. The temperature is calculated using the average value over the drum surface.

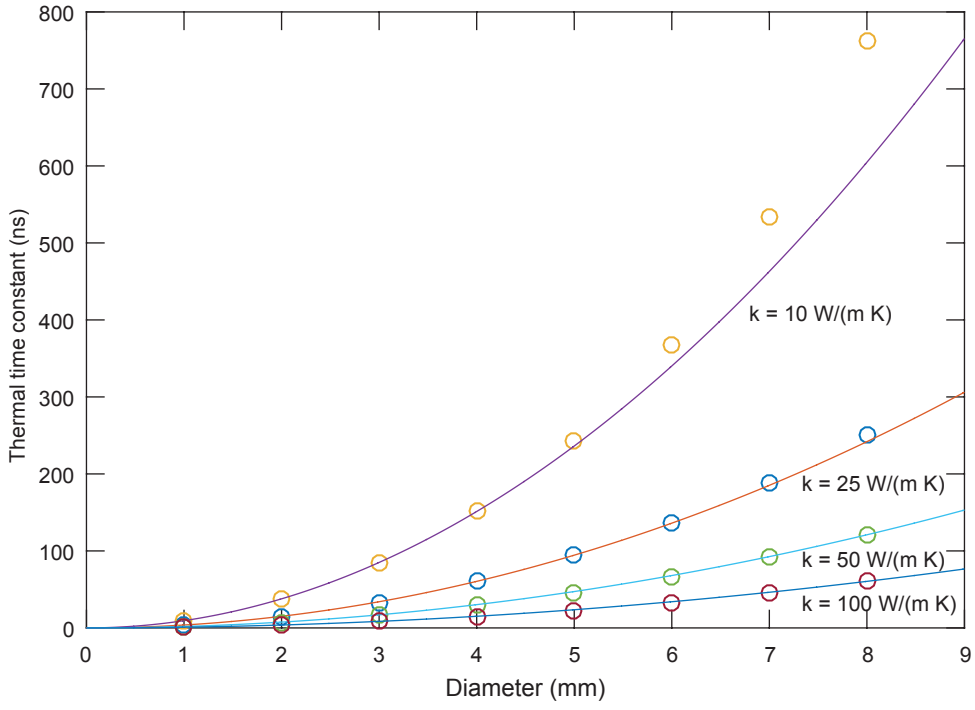

FIG. 3. Diameter dependence of τ for different diameters and different values of k.

Most likely capacitive coupling of the diode laser and photodetector components to the optical table is the cause of this crosstalk. We also found that this feature changes in frequency and amplitude if the mantles of the RF-cables are directly grounded to the table. Our measurement of the parasitic phase shifts in the system cannot correct for this

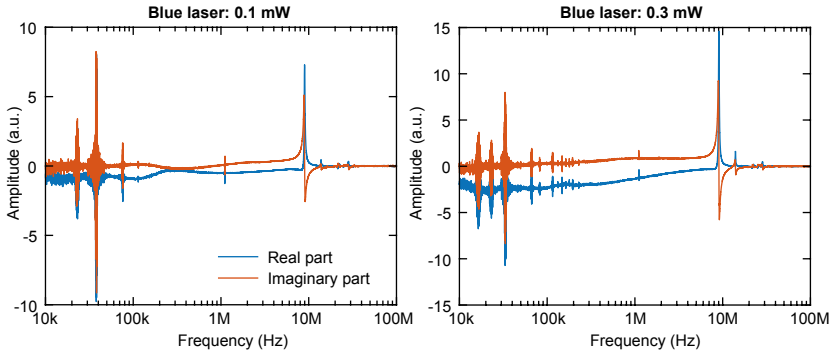

FIG. 4. Additional measurements on single-layer graphene to identify electrical crosstalk. The left figure shows a measurement with exactly the same blue and red laser powers as the experiments with MoS_2. On the right, the neutral density filter behind the blue laser was changed to change the power to 0.3 mW. The electrical cross-talk feature between 100 kHz and 1 MHz diminishes due to the higher optical gain.

effect, because it involves a parallel path to the optical path. Increasing the optical power would reduce this effect, but results in failure of the MoS_2 drums. However, the MoS_2 drums show a much larger signal compared to graphene at the same laser powers, meaning that the magnitude of electrical cross-talk is already less in these drums and the effect is easily accounted for by selecting proper frequency windows for fitting.

AFM CHARACTERIZATION OF CONTAMINATION

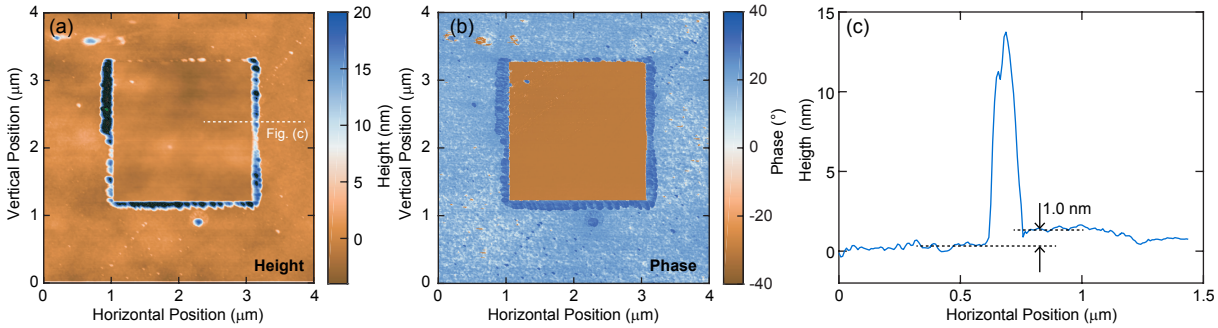

FIG. 5. Characterization of contamination using mechanical cleaning in an atomic force microscope (AFM). (a) Height scan obtained by tapping mode AFM of the 2 by 2 microns area scanned by contact-mode AFM. The white dashed line indicates the trace taken to estimate the height of the contamination. (b) Phase channel of the tapping mode scan, this shows more clearly than the height channel that the scanned area has reduced roughness, indicating that the scanned area has indeed been cleaned. (c) Height profile to estimate the thickness of the contamination, we find the height difference between the cleaned part and the sample to be approximately 1 nm.

In order to characterize contamination of the sample which can influence the experimental results, we use mechanical cleaning by contact mode AFM[2]. A 2 by 2 microns area was scanned with a velocity of 8 μm/s, after which the area was inspected by tapping mode AFM as shown in Fig. 5(a). A square of contamination can be seen around the area that was scanned using contact mode AFM. Inside the square, we find a mean roughness $R_a = 0.73$nm and outside the square we find $R_a = 1.76$ nm. The reduction of roughness is more visible in the phase channel shown in Fig. 5(b). The reduction of roughness inside the square is an indication that we indeed cleaned the sample. Comparing the heights inside and outside the square in Fig. 5(c), we find that the contaminants form a layer approximately 1 nm thick.

To order to study the effect of the contaminants on the transient heat transport of the drums, we attempted to clean 14 drums on the same single layer MoS_2 flake shown in Fig. 7(a). On the suspended drums, a soft cantilever was used for contact-mode AFM to prevent breaking of the suspended drums. After scanning, a stiffer cantilever was used to inspect the area with tapping-mode AFM. Figure 6(a) shows an optical image of the flake after mechanical cleaning, close to the drums the contamination at the borders of the scanning area is visible, but no significant change

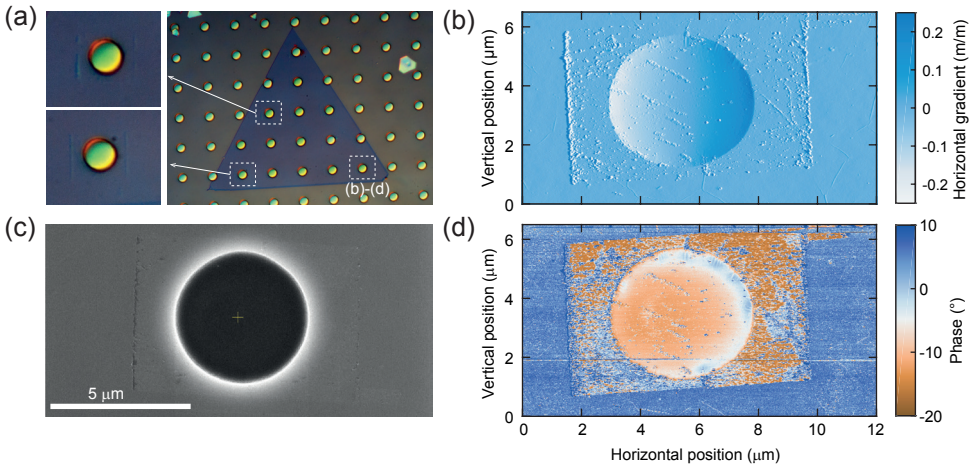

FIG. 6. Characterization of the drums after mechanical cleaning using contact-mode AFM. (a) Optical image of the flake using differential interference contrast microscopy, showing contamination towards the sides of the scanning area. Image was obtained using the raw camera output and automatic enhancement of the contrast in Adobe Photoshop. (b) Gradient of the height channel in the horizontal direction obtained in tapping-mode AFM on drum 14 after cleaning. (c) Scanning electron microsope image of drum 14, the scanned area appears somewhat brighter and contamination on the borders of the contact mode scanning area is visible. (d) Phase channel of the tapping mode AFM. A significant difference in phase is detected in the area scanned by contact mode.

in optical contrast is observed. In scanning electron microscopy in Fig. 6(c) a slight change in contrast is observed, as the cleaned area is slightly brighter. Tapping mode AFM of the drums reveals that some contamination remains after the scan as shown in Figs. 6(b) and (d). Although the scan settings are the same as the smaller test area in Fig. 5, more residue is visible in the phase channel. This could be due to the large height variations, because the drums are deflected downwards by approximately 200 nm due to air pressure in the environment. Nevertheless, a significant portion of the contamination should be removed as evidenced by the pileup of contamination at the sides (Figs. 6(a) and (b)), the contrast in the electron microscopy (Fig. 6(c)) and the phase channel in Fig. 6(d).

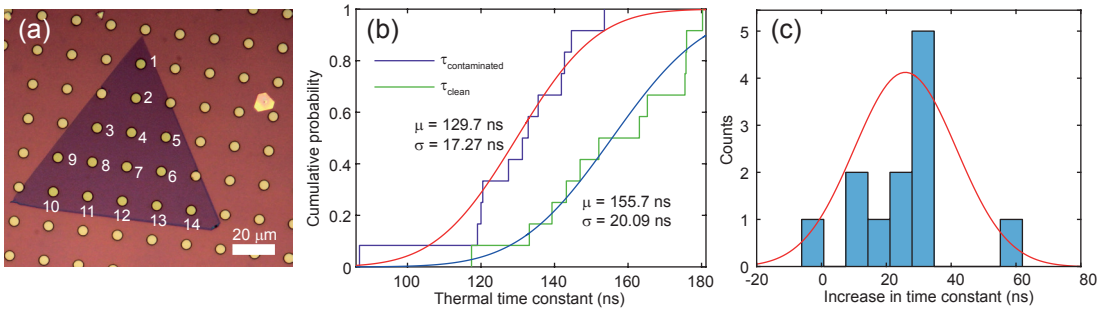

FIG. 7. Thermal characterization before and after mechanical cleaning of suspended drums. (a) Optical image of the flake with the numbers corresponding to table I. (b) Cumulative probability of the thermal time constant before and after mechanical cleaning. (c) Histogram of the increase in thermal time constant.

Due to the low permeability of the drums there is no significant air leakage during the AFM scan, allowing us to immediately measure the thermal time constants after cleaning the sample while the cavity remains in vacuum. The thermal time constants before and after cleaning are shown in Table I, the corresponding drum numbers are labeled in Fig. 7(a). Taking the cumulative probability in Fig. 7(b), we find a significant increase of the mean of the time constants by 26 ns on average (Fig. 7(c)). The device-to-device spread did not decrease significantly, as the standard deviations are similar. The contamination of the drums thus induces a systematic error of approximately 20% in single layer drums with a 5 micron diameter, this is however relatively small compared to the device-to-device spread observed in this work.

TABLE I. Thermal time constants of the single layer MoS_2 drums in Fig. 7(a) before and after mechanical cleaning using contact mode AFM. (*Drum broken during AFM)

Drum	τ before cleaning (ns)	τ after cleaning (ns)	$\Delta\tau$ (ns)
1	108	-*	
2	120	133	13,2
3	154	152	-1,5
4	145	175	30,9
5	133	165	32,4
6	161	150*	
7	142	176	33,9
8	143	176	33,2
9	87	117	30,5
10	136	163	27,5
11	131	139	8,1
12	127	147	19,5
13	120	143	22,7
14	119	180	61,2

* R.J.Dolleman@tudelft.nl

[1] Keith Lewis Aubin, "Radio frequency nano/microelectromechanical resonators: Thermal and nonlinear dynamics studies." (2004).

[2] AM Goossens, VE Calado, A Barreiro, K Watanabe, T Taniguchi, and LMK Vandersypen, "Mechanical cleaning of graphene," Applied Physics Letters **100**, 073110 (2012).